Numerical Modelling Co-Firing Combustion in the Existing Coal-Fired Power Plant: Case Study in Paiton 9 Power Plant

Chairunnisa
Research Center for Energy Conversion and Conservation, National Research and Innovation Agency

Muhammad Penta Helios
Research Center for Energy Conversion and Conservation, National Research and Innovation Agency

Andini, Ade
Research Center for Process and Manufacturing Industry Technology, National Research and Innovation Agency

Agus Prasetyo Nuryadi
Research Center for Energy Conversion and Conservation, National Research and Innovation Agency

他

https://doi.org/10.5109/7236903

出版情報：Evergreen. 11 (3), pp.2638-2649, 2024-09. 九州大学グリーンテクノロジー研究教育センター
バージョン：

Numerical Modelling Co-Firing Combustion in the Existing Coal-Fired Power Plant: Case Study in Paiton 9 Power Plant

Chairunnisa[1], Muhammad Penta Helios[1,*], Ade Andini[2], Agus Prasetyo Nuryadi[1], Achmad Maswan[1], Himawan Sutriyanto[1], Hariyotejo Pujowidodo[1], Bambang Teguh Prasetyo[1], Ariyana Dwiputra Nugraha[3], Nur Cahyo[3]

[1]Research Center for Energy Conversion and Conservation, National Research and Innovation Agency, South Tangerang 15314, Indonesia

[2]Research Center for Process and Manufacturing Industry Technology, National Research and Innovation Agency, South Tangerang 15314, Indonesia

[3]PLN Research Institute, South Jakarta 12760, Indonesia

*Author to whom correspondence should be addressed:
E-mail: muhammad.penta.helios@brin.go.id;

(Received May 8, 2024: Revised June 24, 2024: Accepted August 2, 2024).

Abstract: Biomass cofiring, a technique that involves combusting biomass alongside fossil fuels in power generation, presents a promising pathway toward achieving net-zero emissions. As an alternative solution, biomass co-firing is planned to be implemented to reduce emissions of the existing coal-fired power plant (CFPP) in Indonesia. This paper presents a numerical study using the computational fluid dynamics (CFD) approach. A Paiton 9's power plant was selected as the object domain, and five cases related to fuel composition were prepared i.e., 100% coal, 100% biomass and three cases of mixture ratio of coal and biomass. Sawdust, a source of biomass, is mixed with coal and varies in ratios namely 5%, 10% and 15%. The combination of the species transport model, realizable k-ε turbulence model, combustion model and dual heat exchanger model was used to analyze combustion characteristics such as the average temperature profiles, velocity profiles and mass fractions of pollutants, including NO_x, CO_2, and HC_n. The results report the highest average furnace gas exit temperature is about 1300°C by using 100% coal. By increasing the ratio of sawdust in the coal, the furnace gas exit temperature reduces close to recommended optimum range of gas exit temperature. Furthermore, the NO_x and CO_2 emissions trend to decline due to effects of decreasing furnace temperature and low carbon levels in fuel. Hence, selecting an appropriate sawdust ratio in the coal and fuel composition is the key point to maintaining the stability of furnace exit gas temperature. Later, observations of co-firing combustion are required to ensure the accuracy of the model in this study.

Keywords: cofiring; biomass; emission; realizable k-ε turbulence model; computational fluid dynamics

1. Introduction

Coal combustion is a critical obstacle to achieving net zero emissions due to its high output of carbon dioxide (CO_2). The combustion process also releases pollutants like sulphur dioxide (SO_2), nitrogen oxides (NO_x), particulate matter (PM), heavy metals and black carbon (BC) into the atmosphere, degrading air quality and harming public health[1)]. As a major source of greenhouse gases, coal significantly contributes to global warming and climate change[2)]. Transitioning to net zero emissions requires reducing reliance on coal by adopting cleaner energy sources, enhancing energy efficiency, and implementing carbon capture technologies[3,4)]. Achieving this transition involves substantial policy changes, technological advancements, and coordinated global efforts to mitigate the environmental and health impacts of coal combustion[5,6)].

Indonesia is one of South-East Asia (SEA) countries, which has numerous sources of energy such as crude oil, natural gas, coal, hydro, and renewable energy. The abundant amount of energy sources has supported Indonesia's energy production to satisfy domestic market demand. The energy source conversion is mostly used in petrochemical, transportation, household, and electrical industries. In terms of electricity, coal has a significant contribution to sufficient Indonesian national electricity from 2012 to 2022. During that period, the average

electricity growth from coal sources reaches 22.75%[7]. In 2022, 62.41% of Indonesian electricity is still dominated by coal conversion, followed by combined steam-gas, 18.13% and hydro, 7.17% respectively[8]. Most power plants in Indonesia utilize pulverized coal combustion as their primary method of operation and it is associated with substantial air pollution[9]. As a result, it contributes more than 40% of total emissions in the energy sector[10]. It directly contributed to the greenhouse effect - trapping outgoing infrared radiation and warming the Earth's surface and atmosphere; absorbing and scattering solar radiation - reducing sunlight reaching the Earth's surface and disrupting regional and global climate patterns[11,12]; and increasing Earth's surface temperature - intensified heat retention exacerbates temperature extremes[13,14].

According to the Net-Zero Emissions (NZE) initiative, reducing greenhouse gas emissions and ensuring the sustainability of energy resources are critical priorities. The primary goal of this program is to mitigate the adverse effects of climate change, to address related health issues and to sustain human necessities simultaneously. Controlled climate change and health issues, leading to changes in agricultural productivity and water resources, which was affected human necessities such as food security, water availability, and shelter[15]. By achieving these targets, the program aims to create a balanced and sustainable environment.

Indonesia targeted to achieve the NZE goal by 2060 by promoting Indonesia's Long-Term Strategy for Low Carbon and Climate Resilience 2050 (Indonesia LTS-LCCR 2050)' program[16]. The program focuses on economic development and environmental preservation coexist seamlessly, creating a legacy of sustainability for future generations. As a legal act, Indonesia plans to reduce the use of coal in the energy production sector especially electricity by implementing co-firing biomass. Biomass is being utilized as a viable and environmentally friendly energy source, serving as an alternative to finite and non-renewable energy resources. It can be effectively transformed into electrical energy and thermal energy, thereby catering to the energy demands of residential and industrial domains[8].

As an agricultural nation, Indonesia possesses a diverse and plentiful biomass supply. Indonesia has 130 million tonnes of biomass energy potential. This is equivalent to about 39 Mtoe of energy. About 73% of the potential biomass is derived from agriculture and forest wastes [17]. The assessment of biomass potential was also conducted in 33 provinces in Indonesia. It was revealed that biomass potential was dominated by palm oil and rice husk respectively[18]. About 13 GW of 37.7 GW energy capacity of biomass was gained from palm oil plantations, which has been planned to be converted to electricity of about 2.2 GW in 2022[19]. The proper utilization of biomass as a fuel has been shown to have the potential to decrease emissions, as evidenced by studies[20–23].

Nevertheless, certain challenges are linked to the practice of biomass co-firing. The availability and consistent supply of biomass might pose significant challenges[24–27]. The successful implementation of co-firing projects may necessitate the establishment of supportive laws, incentives, and regulations[28–30]. Biomass feedstocks exhibit distinct features in comparison to coal, encompassing diverse attributes such as fluctuating moisture content, particle size, and energy content. The attainment of a stable and homogeneous fuel mixture while utilizing coal might present difficulties, which in turn can have an impact on combustion efficiency, emissions, and the overall performance of the plant [31–34]. Moreover, biomass ash may exhibit elevated levels of alkali and chlorine content, which can result in the corrosion and fouling of equipment[35,36].

The co-firing of biomass and coal necessitates the implementation of adjustments to pre-existing power plants or industrial boilers to handle the distinct fuel characteristics. Hence, it is imperative to perform a comprehensive investigation to ascertain the combustion attributes of co-firing. This necessitates the undertaking of computational combustion studies that offer precise and cost-effective predictions of combustion processes [37]. The numerical simulation technique has undergone significant advancements, enabling the gathering of data about pulverized coal combustion to predict both combustion and pollution. A study was conducted to investigate the reduction of NO_x and CO emissions in co-firing combustion utilizing the Kobayashi model and kinetics/diffusion-limited rate models. Computational Fluid Dynamics (CFD) was employed as the methodology for this investigation[38]. A study including numerical analysis investigated the co-firing of torrefied biomass, which resulted in notable reductions in CO_2 and NO_x emissions[39]. The investigation and computational analysis of a co-firing system utilizing woody biomass exhibited satisfactory proportions, resulting in a reduction of CO_2 emissions[40]. The study investigates the combustion process of coal and sawdust mixture containing NO_x and SO_x reduction agents, along with biomass derived from corn, wheat, and soybean. The experiments are conducted in a tangentially fired boiler operating at partial loads, as described in reference[41].

To the best author's knowledge, there were limited studies of co-firing combustion through the existing power plant, especially in Indonesia. The present work focuses on investigating the effect of co-firing combustion ratio on flow field and emission e.g., CO_2, NO_x, and HC_n, in the existing coal-fired power plant. CFD is employed to identify flow field behaviour and to analyse emissions trends at end of boiler zone. The results provide useful information regarding the best ratio of cofiring for emissions reduction as well as new renewable energy utilization.

2. Data Collection and Reduction

2.1 Technical Data

This study encompasses the provision of boiler technical drawings and the presentation of the arrangement of boiler components, together with their respective measurements. One of the technical illustrations is a representation that depicts a cross-section. The technical data is required to generate a simulation domain which represents the simplification of actual boiler geometry. The boiler from Paiton 9 with a capacity of 660 MW was used in this simulation. In general, the dimension of domain is 41.66 m × 20.03 m × 69.26 m, meanwhile the details of the heat exchanger, burner and other components are provided in our previous report[42]. Subsequently, the software can be utilized to simulate the boiler's behaviour by incorporating relevant process data.

2.2 Operational Data

The operational data is required to define initial and boundary conditions for the model. Adequate data and proper setup lead to a good prediction of the results. In this case, the data encompassing flow rate and temperature of air and fuel is essential to be collected. The flowrate and temperature of each stream were set by following data in Table 1. The aforementioned data is used to estimate the required quantity of fuel and air for each burner.

Table 1. Fuel and air flow rates and temperature of Paiton 9 CFPP[42].

Flow rate	$\dot{m}$ (kg/s)	$\dot{m}$ (T/h)	T (°C)
Primary air	100.86	363.10	199
Coal	48.85	175.85	52.2
Secondary air	261.01	939.65	340

In addition, the data related to heat absorption of the flame or the combustion gas by heat exchanger is compulsory. The data is purposed for evaluating the performance of the boiler through the comparison of measurement outcomes during its operational state. The input data for the heat exchanger is summarized in Table 2.

Table 3 shows the matrix of cofiring fuel used in the boiler combustion. There are five cases related to fuel composition prepared i.e., 100% coal, 100% biomass and three cases of mixture ratio of coal and biomass. Sawdust, a source of biomass, is mixed with coal and varies in ratios namely 5%, 10% and 15%.

Table 2. Input data of fluids in the heat exchanger zone[42].

Heat Exchanger	Abbreviation	Fluid	Flowrate (kg/s)	Temperature (°C)
Cold Superheater	C-SH	High pressure steam	220.61	347.00
Division Panel Superheater	DPSH	High pressure steam	226.69	422.30
Larger Platen Superheater	P-SH	High pressure steam	235.28	433.88
Final Superheater	F-SH	High pressure steam	236.14	501.35
Intermediate Reheater	I-RH	Medium pressure steam	208.33	337.65
High Reheater	H-RH	Medium pressure steam	221.25	251.23
Economizer	ECO	Water liquid	227.03	269.60

Table 3. Matrix of co-firing combustion.

Mixed	Mass Fraction (%)	Sawdust				
		0	5	10	15	100
Coal	0					100B
	85				85C15B	
	90			90C10B		
	95		95C5B			
	100	100C				

Further, the mixture of coal and sawdust affects the reduction of carbon level as well as increasing moisture and volatile matter. The mixture of coal and sawdust also influenced the composition of fuel i.e., C and volatile matter, the heating value and density of fuel were affected as well. Hence, Dulong's formula for solid fuels is used to determine the heating value of fuels, while the density of the mixture is calculated by comparing each mass fraction. The ultimate and proximate analysis of fuel was tabulated in Table 4.

Table 4. Fuel composition.

Component	Composition Value				
	100C	95C5B	90C10B	85C15B	100B
Ultimate analysis (DAF, wt. %)					
C	46.38	45.46	44.55	43.63	28.06
H	3.41	3.40	3.39	3.37	3.17
N	0.81	0.78	0.74	0.71	0.15
S	0.2	0.19	0.19	0.18	0.07
O	13.32	13.89	14.47	15.04	24.8
Proximate analysis (As Received, wt. %)					
Moisture	31.92	32.41	32.90	33.39	41.74
Ash	4.14	4.03	3.93	3.82	2.01
Volatile	33.04	33.70	34.36	35.02	46.25
Fixed C	31.07	30.02	28.96	27.91	10
N (DAF)	0.01267	0.01223	0.01178	0.01133	0.00267
Density (kg/m³)	1400.00	1192.14	1038.02	919.19	312.00
HHV (kJ/kg)	17355.16	17051.25	16747.35	16443.45	11277.08

3. CFD Modelling Setup

The SIMPLE algorithm as the solution method was applied to solve the RANS equation. The second order of spatial discretization was applied to solve pressure, momentum, and energy terms simultaneously. Later, the convergence criteria of all calculations are accepted when the residuals of all variables are less than 10^{-4} and the mass balance difference of each case is less than 1%. The sequences of the simulation were described as follows.

3.1 Governing Equations

The continuity, momentum and energy equations used in this study were written to equations 1 to 3 respectively [43–45].

$$\frac{\partial \rho}{\partial t} + \nabla.(\rho\,\vec{u}) = 0 \tag{1}$$

$$\frac{\partial}{\partial t}(\rho\vec{u}) + \nabla.(\rho\vec{u}\vec{u}) = 0 \tag{2}$$

$$-\nabla \mathrm{p} + \nabla.(\bar{\bar{\tau}}) + \rho\vec{g} = 0 \tag{3}$$

where p is the static pressure, $\bar{\bar{\tau}}$ is the stress tensor, ρ is the density of fluid and $\vec{g}$ is the gravitational body force. Later, S_h is the source of chemical reaction energy:

$$S_h = -\Sigma\frac{h_j^0}{M_j}R_j \tag{4}$$

H is the total enthalpy:

$$H = \sum_j Y_j H_j \tag{5}$$

3.2 Discrete Phase Model (DPM)

Discrete Phase Model (DPM) trajectory coal:

$$m_p\frac{d\vec{v}_p}{dt} = \Sigma\vec{F} \tag{6}$$

where m_p, $\vec{v}_p$, and $\vec{F}$ are defined as particle of mass, relative velocity of particle and external force respectively. The force balance accounts for the particle inertia with the forces acting on the particle. On the right side, the first term is the drag force per unit particle mass, second term is a gravity term. Hence the total force of the particle is drag and buoyancy forces. This leads to a specific equation of motion [46].

$$\frac{g(\rho_p-\rho)}{\rho_g}\frac{d\vec{v}_p}{dt} = F_D(\vec{v}-\vec{v}_p) + \frac{g(\rho_p-\rho)}{\rho_g} \tag{7}$$

Since the drag force occur on particle, the relative Reynold number required to estimate due to its effect. Here, $\vec{v}_p$ is the particle phase velocity, $\vec{v}$ is the fluid phase velocity, μ is the molecular viscosity of the fluid, ρ_p is the density of the particle, and d_p is the particle diameter. Re_p describes the relative particle Reynolds number, while C_D represents the drag coefficient [46].

$$Re_p = \left(\frac{\rho d_p|\vec{v}_p-\vec{v}|}{\mu}\right) \tag{8}$$

$$C_D = \frac{24}{Re}(1+11.2355Re^{0.653}) + \frac{(-0.8271)Re}{8.8798+Re} \tag{9}$$

3.3 Turbulence & Radiation Models

The equation used to transport turbulent kinetic energy (K) and turbulent effects were considered by utilizing the realizable k-ε turbulent model as follows [47]:

$$\frac{\partial(\rho k)}{\partial t} + \nabla.(\rho\vec{u}k) = \nabla.\left[\left(\mu+\frac{\mu_t}{\sigma_k}\right)\nabla k\right] + G_k - \rho\varepsilon + P_K \tag{10}$$

The realizable k–ε model was chosen because of its superior performance in predicting the behaviour of jets and swirling flows compared to the ordinary k–ε model [48]. The results of this study indicate that this model exhibited superior convergence in comparison to the renormalized group (RNG) k–ε model [49]. Later, the radiation of flame during combustion was modelled using the Discrete Ordinates (DO) model as given as follows[50]:

$$\nabla.(I_\lambda(\vec{r},\vec{s})\vec{s}) + (a_\lambda+\sigma_s)I_\lambda(\vec{r},\vec{s}) = a_\lambda n^2 I_{b\lambda} + \frac{\sigma_s}{4\pi}\int_0^{4\pi} I_\lambda(\vec{r},\vec{s}')\varphi(\vec{s},\vec{s}')d\Omega' \tag{11}$$

3.4 Dual-Cell Heat Exchanger Model

A dual-cell model is employed to replicate heat transfer. This model effectively illustrates the temperature distribution in both the primary and auxiliary flows, without being restricted by mesh type or heat exchanger geometry [51]. This model could be used to model compact tube heat exchanger for aero engines as well [52]. In this study, the simulation incorporates dual cell heat exchanger

models to represent the superheater, panel superheater, final superheater, medium reheater, final reheater, and economizer. Based on this rationale, additional fluid is designated as a novel substance, specifically "steam-sh" for the fluid in the superheater section, "steam-rh" for the reheater section, and water liquid for the fluid in the economizer section. Unlike conventional heat exchangers, division superheater panels are not classified as heat exchangers (HE). Instead, they are characterized as solid structures with a specific temperature and capacity to absorb thermal energy. The utilization of this technique is justified due to the multifunctionality of the division superheater panel. In addition to its primary role as a heat exchanger, it also serves as a flow director, ensuring the uniform distribution of the previously circular flow within the furnace to the convection section.

4. Domain and Grid Preparation

4.1 Discretization

The three-dimensional geometric and mesh model of the Paiton 9's CFPP is depicted in Fig. 1. The heat transfer components (Economiser, Superheater, Reheater) are modelled as Heat Exchanger blocks. In the meantime, the furnace walls and water walls, are modelled as constant-temperature planes. The saturation temperature of the water in the water walls is estimated from pressure in the boiler drum. The opposing wall, referred to as the convection region, is shown as an adiabatic wall, assuming ideal insulation.

Furthermore, the boiler used in the CFPP Paiton 9 employs a tangential firing system. This system involves strategically placing multiple burners in each corner of the furnace in a vertical arrangement, alternating between oil burners and low-rank coal burners. This simulation focuses exclusively on the low-rank coal burners, which are essential for the power plant's operation. The number of burner levels corresponds directly to the number of coal mills, ensuring that each level receives an adequate fuel supply. The operational mechanism distributes powdered coal from each coal mill to four burners located at the same vertical level in the furnace corners. This setup allows for an even and efficient combustion process, as the coal is uniformly distributed and ignited across the furnace. The precise burner placement and fuel distribution optimize performance, reduce emissions, and ensure consistent steam and power generation. The employed mesh models comprise both structured and unstructured meshes. The heat exchanger geometries are constructed using a hexahedral (structured) mesh, which encompasses multiple zones surrounding the heat exchanger. The remaining objects, characterized by more intricate geometry, are converted into unstructured meshes in order to expedite the modelling process. The quantity of meshes within the computation domain is depicted in Fig. 1.

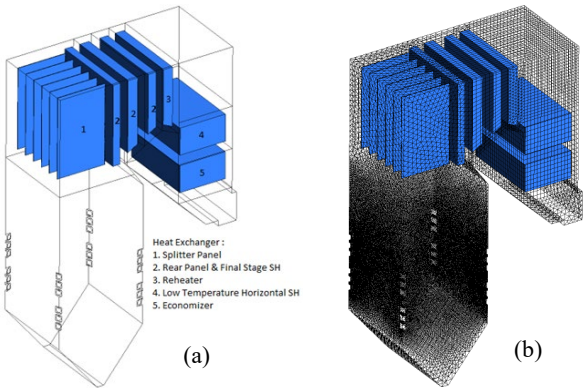

Fig. 1: 3D domain Paiton 9's Coal Fired Power Plant: fluid domain (a) and meshing (b) [42].

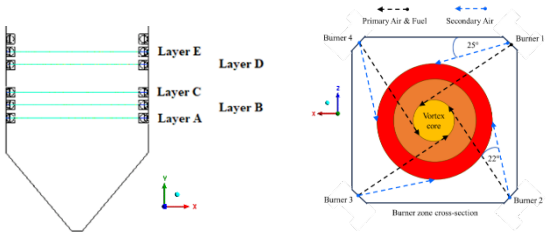

Fig.2: Burner domain: burner layer in the furnace (left) and burner cross-section (right).

The burner geometry is represented by a rectangular planar surface, with a centrally found cylindrical aperture as shown in Fig. 2. The cross-sectional representation of the secondary air route is depicted as a rectangular flat surface, while the primary air channel is represented by a cylindrical hole. The secondary air passage's cross-section is situated at the furnace's corner, inclined at an angle of 25°relative to the furnace's side. The secondary air speed vector is oriented orthogonally to the cross section, while the primary air speed vector exhibits an angular deviation of 22° from the secondary air speed vector.

4.2 Boundary Condition Setup

Proper setups are required to achieve good results and stability during the steady state combustion process. According to the actual condition of the site, there were only five burners used at that time. In this simulation, the mass flow inlet was defined for coal, primary air, and secondary air respectively. The outlet of economizer is set as a pressure outlet. The detailed inlet and outlet settings of tangential boiler were able to be found in the reference [53–57]. The airflow throughout the system, commencing at the Forced Draft Fan (FDF) and progressing via the air heater, burner, furnace, superheater, reheater, and economizer, encounters impediments resulting in the gas exiting the economizer being subjected to vacuum pressure. In order to facilitate the release of gas into the atmosphere, the utilization of Induced Draft Fan (IDF) and chimney systems is necessary. The vacuum pressure value for the Paiton 9 CFPP boiler is -547.7 pascals [41].

4.3 Grid Independence Test

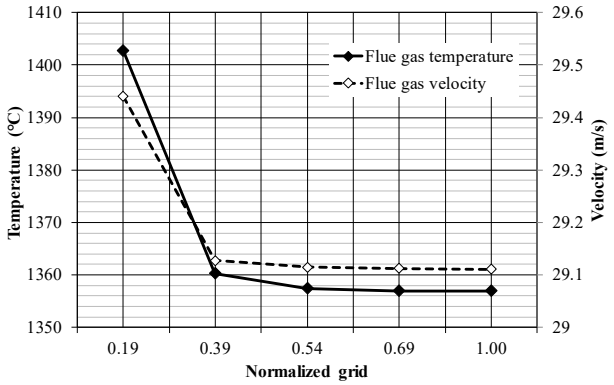

Fig. 3: Grid independence test of flue gas temperature and velocity at furnace exit plane.

Combustion with 100% coal or 100C is used for conducting grid independence. Five grid performance is evaluated, and it is compared to each other number of elements of the grid. The normalized grid – ratio from the largest to the smallest number of elements is adopted to examine the mesh independency [58]. It can be seen that the velocity magnitude and temperature of the flue gas trend at furnace exit position was linear from 0.54 to 1.00. Commonly, the percentage error tends to decrease with the increase of grid quantity [59]. The highest relative errors are identified as 1.06% for velocity and 3.03% for temperature. Then, the error of each grid tends to be smaller from 0.39 to 1.00. However, the normalized grid 0.54 is selected in this study, since it maintains grid independence consistency error about 0.04% for velocity and 0.21 % for temperature. It also affected the decreasing simulation time.

5. Results and Discussion

5.1 Verification and Validation

The combustion temperature in the furnace was selected as a verification parameter. The combustion model validation was compared to the measurement report and manual calculation. The highest adiabatic combustion temperature was assessed ranging from 1250 to 1500°C, and the average flame core temperature was verified at 1480°C at 20 m height of the boiler. It was acceptable since the flame core temperature was about 1500 to 1600 °C [60]. In the case of validation, there were limitations of new data measurement. Hence, the furnace exit gas temperature (FEGT) was selected to be compared with the manual calculation or measurement data in our previous report [41]. The furnace exit gas temperature was estimated to be about 1321°C by assuming the high heating value of coal around 4147 kcal/kg: moisture content of 31.92%, and losses from incomplete combustion and unburned carbon at 3% and 10% respectively [61]. In essence, the discrepancy between CFD results and manual calculation was about 1.59%. Later, the temperatures from the distributed control system (DCS) are required to ensure the high validity of the model.

5.2 Velocity and Temperature Profiles

Prior to combustion, the coal and primary are sprayed from different nozzle channels in certain angles. The fuel from four burners created a vortex due to the particle collision. The high velocity of secondary air flew the coal particles in the furnace zone and its temperature ignited the volatilization of coal. Hence, the temperature in the furnace was rising as well as increasing the turbulence intensity.

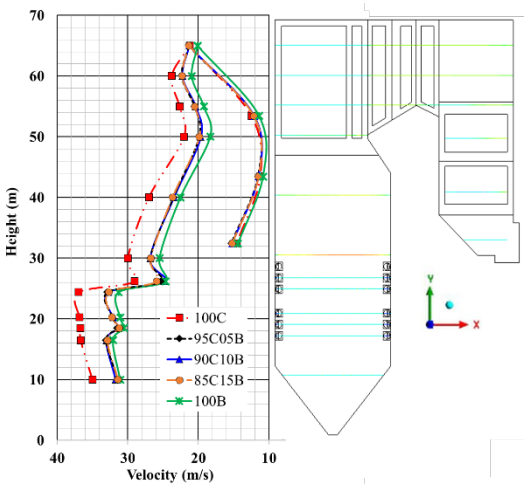

Fig. 4: Velocity profile of average flue gas velocity in the boiler height.

Figure 4 depicts the velocity profile of fluid in the streamwise direction or *xy* plane. Fourteen planes at certain height of the furnace were provided to assess the average velocity of fluid. The streamwise velocity of fluid was identified from the range 18 m/s to 38 m/s in the furnace zone. Later the velocity decreased from 23 m/s to 10 m/s. 100C, or 100% coal combustion led to the highest velocity profile among other solid fuels. Even though fuels 95C05B, 90C10B, 85C15B and 100B have high volatile matter compared to 100C, the velocity was lower due increasing of moisture content in it. As example, both 95C05B and 85C15B volatile matter rises 0.66% and 1.98% respectively. Similarly to moisture content, both increase 0.22% and 1.47% respectively.

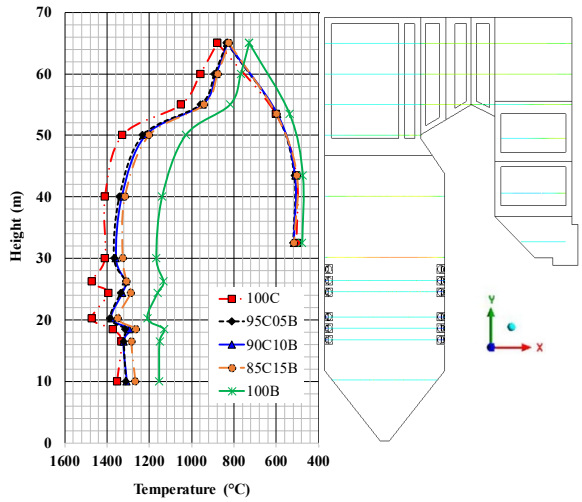

Fig. 5: Temperature profile of average flue gas temperature in the boiler height.

Figure 5 depicts the temperature profile of fluid towards height of boiler. It was identified that coal combustion temperature in the furnace reached about 1300 ºC compared to others. The temperature seems fluctuate above 1400 ºC as shown in the burner layer C and E. The highest combustion temperature reach by coal was clearly due to coal's high heating value, which was caused due to the carbon content in each solid fuel[62,63]. From height 10 m to 50 m, the temperature along furnace decrease. It caused not only by decreasing of heating value of co-firing fuel but also increasing of volatile matter of them. As example, with 5% co-firing ratio or 95C05B, the heating value declines 1.75%, while the heating value decreases 5.25% at 15% co-firing ratio. As mentioned in the preceding section, high volatile matter means the solid fuel was able combusted easy at certain temperature. 85C15B is combusted at average temperature 1298.60 ºC, while 95C05B is combusted at average temperature 1339.25 ºC. Later, the high temperature of exit furnace indicated that flame combustion was required to be maintained following design requirements. The decreasing temperature in the convection zone was caused by heat absorption by heat exchanger arrangements. In addition, mixing between coal and sawdust affects temperature distribution in the boiler, especially in furnace zone. For example, adding 5 to 15% sawdust decreases the flame core temperature about 50 ºC to 100 ºC. However, the decrease depended on the moisture content in the sawdust. In the end, the temperature of flue gas exiting the end zone of the economizer was identified about 500 ºC, which is no significant difference for other solid fuels.

To keep the convection zone, clean from slagging and fouling, the exit furnace gas temperature must be controlled in the range of ash fusion temperature about 1100 ºC -1400 ºC[64,65] for low rank coal and 1200 ºC -1500 ºC for high rank coal[66]. The furnace exit gas temperature of 100% coal combustion was well predicted via CFD simulation as shown in Fig. 6. However, the preferred temperature of low rank coal combustion is lower the bottom limit of FEGT or less than 1100 ºC.

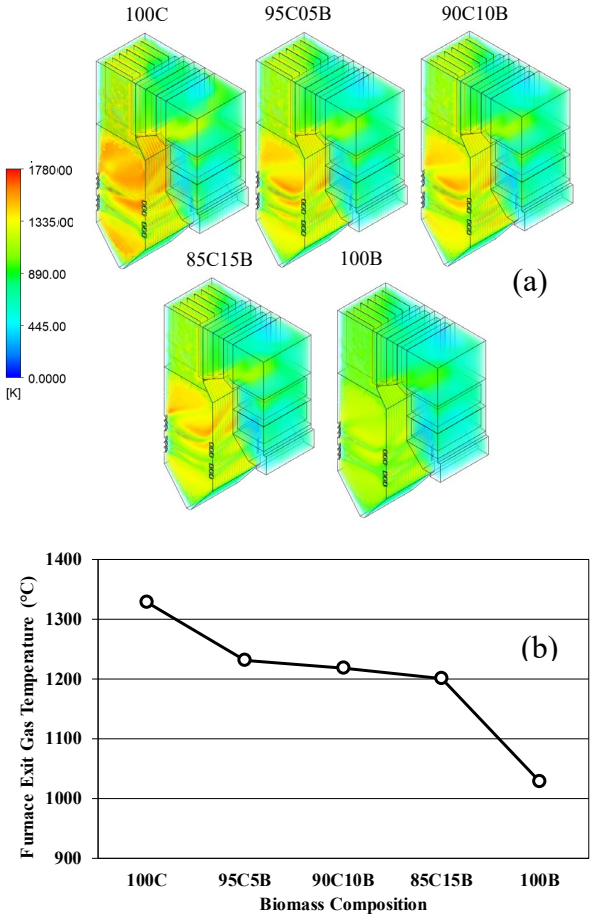

Fig. 6: Iso-volume temperature distribution (a) and average furnace exit gas temperature (b).

There are two methods to decrease the observed temperature peak and hence minimise the maximum local radiative heat flow in the upper section of the furnace. To maintain a steady total combustion air flow rate, one can either increase the secondary air flow rate or decrease the flow rate and change the tilt angle of Over Fire Air (OFA)[67,68]. In addition, the upper furnace temperature tended to decrease by increasing the ratio of sawdust in coal. Based on the iso volume contour, the simulation found the highest temperature was at initial ignition.

5.3 Combustion Products

Blending biomass, such as wood pellets or agricultural residues, with traditional coal or natural gas in combustion processes, the carbon footprint of energy production can be significantly diminished. Biomass is considered carbon neutral as the carbon dioxide released during combustion is roughly equivalent to the amount absorbed by plants during their growth, creating a closed carbon cycle. As a greenhouse gas element, it significantly contributes to the greenhouse effect, global warming, and climate change. Elevated CO_2 levels lead to disruptions in ecosystems,

altered weather patterns, ocean acidification, and rising sea levels, posing threats to biodiversity and human societies. Figure 7(a) shows release of CO_2 trend after combustion. By mixing the sawdust into the coal, it significantly affects the CO_2 reduction[69]. The present study disclose that the CO_2 mole fraction of coal was estimated at around 0.09 at 100C case and 0.069 at 100B case. The CO_2 emission was reduced about 3.33 % by increasing 15% of sawdust or at 85C15B case. However, the effect of sawdust addition on heat input and power generation output is required to be considered during the process. Mitigating these impacts to reduce CO_2 emissions through the adoption of cleaner energy sources such as carbon capture and storage (CCS) aims to capture CO_2 before release.

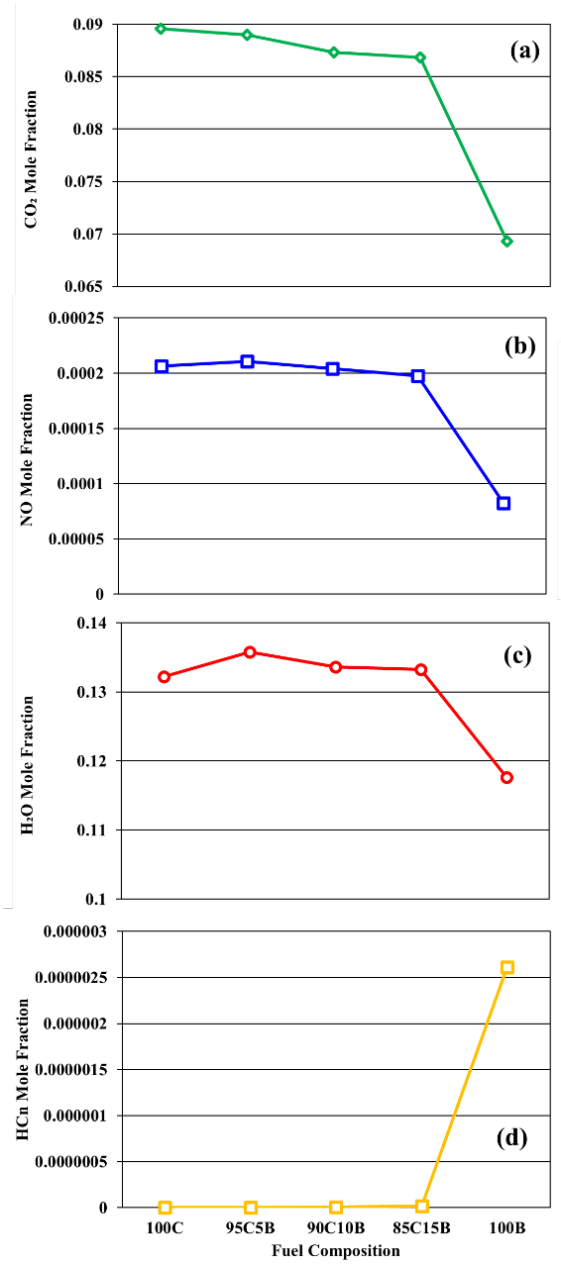

Fig. 7: Mole fraction of combustion products based on mixture ratio of coal and sawdust.

Figure 7(b) depicts declining the trend regarding nitrogen oxides (NO_x), including nitrogen dioxide (NO_2) and nitric oxide (NO). It can vary depending on the specific conditions and characteristics of the solid fuel mix NO_x emissions are a concern in combustion processes as they contribute to air pollution and can have adverse environmental and health effects. The impact on NO_x emissions during co-firing can be influenced by factors such as the nitrogen content of the sawdust, combustion temperature, and the presence of nitrogen-containing compounds in the fuel mix. Sawdust generally contains combustion of it tends to occur at lower temperatures, which can mitigate NO_x formation[70].

The present simulation reveal that the NO_x mole fraction of coal was estimated around 0.00205 or equivalent to 251.45 mg/m^3 at 100C case and around 98.13 mg/m^3 at 100B case. The present value was in good agreement with the previous NO_x prediction by Chang[71]. Hence, the NO_x emission reduces about 9.52% by increasing 15% of sawdust or at 85C15B case. However, the effect of sawdust addition on heat input and power generation output is required to be considered during the process.

The moisture content of sawdust in co-firing can significantly influence the combustion process and overall system efficiency. The Sawdust typically contains a certain amount of moisture, and the presence of water vapor during combustion can affect several aspects of the process such as, ignition and combustion efficiency: flue gas composition and heat output[72]. Some of the moisture of sawdust evaporates into vapour form, but it depends on the heat released from the combustion. Figure 7(c) shows steam vapor decline during the increase of co-firing ratio.

Figure 7(d) shows the appearance of hydrogen cyanide (HC_n) during the combustion. Significant quantities of nitrogen oxides (NO_x and N_2O) are produced by the conversion of nitrogen found in coal as well as in sawdust. HC_n and ammonia (NH_3) serve as intermediate compounds in the reaction. HC_n and NH_3 are released during the process of devolatilization, which takes place at the early stages of combustion[73,74]. HC_n is a transparent or light-blue substance in liquid or gaseous form that emits a bitter scent resembling almonds. Hydrogen cyanide disrupts the body's utilization of oxygen and can potentially inflict damage to the brain, heart, blood vessels, and lungs. Exposure has the potential to cause death[74–76]. In case of boiler, there are no significant problem reports the effect of HC_n on steel. However, other research claims that HC_n reacted to specific metals i.e. gold, silver and copper and formed a layer on the surface[77]. Regarding the present simulation, the HC_n might be at high risk on human health compared to boiler performance.

6. Conclusion

The present study performed numerical simulations to investigate combustion performance, flow fields and gas production during cofiring ratios in existing coal-fired

power plant (CFPP). The simulations considered different ratios of sawdust to coal. The results showed that when 100% coal was burned, the model matched well with actual combustion. The power output and temperature were measured for a 100% coal case, producing 660MW at a furnace exit gas temperature of 1321°C. Introducing sawdust into the mix reduced both emissions (NO_x and CO_2) and power output, while increasing HC_n fraction. To maintain stable power output, an optimal mixing ratio of sawdust and coal needs to be determined. By assuming the efficiency of turbine about 30% as studied by Wahid[78]. The study suggested that with 15% co-firing ratio, the power plant could still generate over 600 MW, but adjusting the sixth burner operation might be needed to compensate for the slight reduction. This approach could help Paiton's 9 CFPP achieve both stable power output and emissions reduction. Further, the statistical analysis was considered to be implemented in the separated manuscript with focus on the relation of combustion temperature, cofiring ratio, and prediction of pollutants in the future. Then, future simulations will explore the best co-firing ratio for coal and biomass to align with Indonesia's long-term low-carbon strategy for 2050 in existing power plants.

Acknowledgements

The authors acknowledge the provision of operating and technical data for Paiton's 9 Power Plant by the State Electric Company of Indonesia, the support grant from the Organization for Energy and Manufacture for the study cofiring biomass and the provided software facilities of the National Research and Innovation Agency of Indonesia.

References

1) T.C. Bond, S.J. Doherty, D.W. Fahey, P.M. Forster, T. Berntsen, B.J. DeAngelo, M.G. Flanner, S. Ghan, B. Kärcher, D. Koch, S. Kinne, Y. Kondo, P.K. Quinn, M.C. Sarofim, M.G. Schultz, M. Schulz, C. Venkataraman, H. Zhang, S. Zhang, N. Bellouin, S.K. Guttikunda, P.K. Hopke, M.Z. Jacobson, J.W. Kaiser, Z. Klimont, U. Lohmann, J.P. Schwarz, D. Shindell, T. Storelvmo, S.G. Warren, and C.S. Zender, "Bounding the role of black carbon in the climate system: a scientific assessment," *J. Geophys. Res. Atmos.*, **118** (*11*) 5380–5552 (2013). doi:10.1002/jgrd.50171.
2) S. Rao, Z. Klimont, S.J. Smith, R. Van Dingenen, F. Dentener, L. Bouwman, K. Riahi, M. Amann, B.L. Bodirsky, D.P. van Vuuren, L. Aleluia Reis, K. Calvin, L. Drouet, O. Fricko, S. Fujimori, D. Gernaat, P. Havlik, M. Harmsen, T. Hasegawa, C. Heyes, J. Hilaire, G. Luderer, T. Masui, E. Stehfest, J. Strefler, S. van der Sluis, and M. Tavoni, "Future air pollution in the shared socio-economic pathways," *Glob. Environ. Chang.*, **42** 346–358 (2017). doi:10.1016/j.gloenvcha.2016.05.012.
3) D. Leeson, N. Mac Dowell, N. Shah, C. Petit, and P.S. Fennell, "A techno-economic analysis and systematic review of carbon capture and storage (ccs) applied to the iron and steel, cement, oil refining and pulp and paper industries, as well as other high purity sources," *Int. J. Greenh. Gas Control*, **61** 71–84 (2017). doi:10.1016/j.ijggc.2017.03.020.
4) G. He, J. Lin, Y. Zhang, W. Zhang, G. Larangeira, C. Zhang, W. Peng, M. Liu, and F. Yang, "Enabling a rapid and just transition away from coal in china," *One Earth*, **3** (*2*) 187–194 (2020). doi:10.1016/j.oneear.2020.07.012.
5) J. Rissman, C. Bataille, E. Masanet, N. Aden, W.R. Morrow, N. Zhou, N. Elliott, R. Dell, N. Heeren, B. Huckestein, J. Cresko, S.A. Miller, J. Roy, P. Fennell, B. Cremmins, T. Koch Blank, D. Hone, E.D. Williams, S. de la Rue du Can, B. Sisson, M. Williams, J. Katzenberger, D. Burtraw, G. Sethi, H. Ping, D. Danielson, H. Lu, T. Lorber, J. Dinkel, and J. Helseth, "Technologies and policies to decarbonize global industry: review and assessment of mitigation drivers through 2070," *Appl. Energy*, **266** 114848 (2020). doi:10.1016/j.apenergy.2020.114848.
6) G.L. Morrison, and Sudjito, "Solar radiation data for indonesia," *Sol. Energy*, **49** (*1*) 65–76 (1992). doi:10.1016/0038-092X(92)90128-W.
7) Ministry of Energy and Mineral Resources (MEMR) of Indonesia, "Handbook of Energy & Economic Statistics of Indonesia 2022," Jakarta, 2022. https://www.esdm.go.id/assets/media/content/content-handbook-of-energy-and-economic-statistics-of-indonesia-2022.pdf.
8) IEA, "World Energy Outlook 2022," France, 2022.
9) L.D. Smoot, and L.L. Baxter, "Fossil Fuel Power Stations—Coal Utilization," in: Encycl. Phys. Sci. Technol., Elsevier, 2003: pp. 121–144. doi:10.1016/B0-12-227410-5/00257-X.
10) M.P. Helios, A. Maswan, R.J. Komara, H. Sutriyanto, B. Nuryadin, and A. Andini, "Energy, exergy, and externalities cost rate analysis of 300 mw coal-fired power plant: a case study," *Maj. Ilm. Pengkaj. Ind.*, **16** (*3*) 103–113 (2023). doi:10.29122/mipi.v16i3.5405.
11) A.H. Ismail, "Prediction of global solar radiation from sunrise duration using regression functions," *Kuwait J. Sci.*, (2021). doi:10.48129/kjs.15051.
12) A. Haj Ismail, E.A. Dawi, N. Almokdad, A. Abdelkader, and O. Salem, "Estimation and comparison of the clearness index using mathematical models - case study in the united arab emirates," *Evergreen*, **10** (*2*) 863–869 (2023). doi:10.5109/6792841.
13) V. Ramanathan, and G. Carmichael, "Global and regional climate changes due to black carbon," *Nat. Geosci.*, **1** (*4*) 221–227 (2008). doi:10.1038/ngeo156.

14) J. Hansen, M. Sato, and R. Ruedy, "Perception of climate change," *Proc. Natl. Acad. Sci.*, **109** (*37*) (2012). doi:10.1073/pnas.1205276109.
15) N. Watts, M. Amann, S. Ayeb-Karlsson, K. Belesova, T. Bouley, M. Boykoff, P. Byass, A. Costello, et al., "The lancet countdown on health and climate change: from 25 years of inaction to a global transformation for public health," *Lancet*, **391** (*10120*) 581–630 (2018). doi:10.1016/S0140-6736(17)32464-9.
16) J. Santosa, Arief Heru Kuncoro, A. Dwijatmiko, Nurry Widya Hesty, and A. Darmawan, "The role of nuclear power plants in indonesia towards net zero emissions (nze) in 2060 with a multi regions approach," *Evergreen*, **10** (*3*) 1660–1673 (2023). doi:10.5109/7151715.
17) E. Erdiwansyah, M. Mahidin, H. Husin, N. Nasaruddin, K. Khairil, M. Zaki, and J. Jalaluddin, "Investigation of availability, demand, targets, and development of renewable energy in 2017–2050: a case study in indonesia," *Int. J. Coal Sci. Technol.*, **8** (*4*) 483–499 (2021). doi:10.1007/s40789-020-00391-4.
18) Mahidin, Saifullah, Erdiwansyah, Hamdani, Hisbullah, A.P. Hayati, M. Zhafran, M.A. Sidiq, A. Rinaldi, B. Fitria, R. Tarisma, and Y. Bindar, "Analysis of power from palm oil solid waste for biomass power plants: a case study in aceh province," *Chemosphere*, **253** 126714 (2020). doi:10.1016/j.chemosphere.2020.126714.
19) A. Saputra, B. Sriyono, and L. Pauling, "Mini review of indonesia's potential bioenergy and regulations," *IOP Conf. Ser. Earth Environ. Sci.*, **997** (*1*) 012004 (2022). doi:10.1088/1755-1315/997/1/012004.
20) M. Saleem, "Possibility of utilizing agriculture biomass as a renewable and sustainable future energy source," *Heliyon*, **8** (*2*) e08905 (2022). doi:10.1016/j.heliyon.2022.e08905.
21) D.R. Farine, D.A. O'Connell, R. John Raison, B.M. May, M.H. O'Connor, D.F. Crawford, A. Herr, J.A. Taylor, T. Jovanovic, P.K. Campbell, M.I.A. Dunlop, L.C. Rodriguez, M.L. Poole, A.L. Braid, and D. Kriticos, "An assessment of biomass for bioelectricity and biofuel, and for greenhouse gas emission reduction in <scp>a</scp> ustralia," *GCB Bioenergy*, **4** (*2*) 148–175 (2012). doi:10.1111/j.1757-1707.2011.01115.x.
22) Y. Sung, S. Lee, C. Kim, D. Jun, C. Moon, G. Choi, and D. Kim, "Synergistic effect of co-firing woody biomass with coal on nox reduction and burnout during air-staged combustion," *Exp. Therm. Fluid Sci.*, **71** 114–125 (2016). doi:10.1016/j.expthermflusci.2015.10.018.
23) M. Rehfeldt, E. Worrell, W. Eichhammer, and T. Fleiter, "A review of the emission reduction potential of fuel switch towards biomass and electricity in european basic materials industry until 2030," *Renew. Sustain. Energy Rev.*, **120** 109672 (2020). doi:10.1016/j.rser.2019.109672.
24) J. Popp, S. Kovács, J. Oláh, Z. Divéki, and E. Balázs, "Bioeconomy: biomass and biomass-based energy supply and demand," *N. Biotechnol.*, **60** 76–84 (2021). doi:10.1016/j.nbt.2020.10.004.
25) M.S. Roni, S. Chowdhury, S. Mamun, M. Marufuzzaman, W. Lein, and S. Johnson, "Biomass co-firing technology with policies, challenges, and opportunities: a global review," *Renew. Sustain. Energy Rev.*, **78** 1089–1101 (2017). doi:10.1016/j.rser.2017.05.023.
26) D.S. Primadita, I.N.S. Kumara, and W.G. Ariastina, "A review on biomass for electricity generation in indonesia," *J. Electr. Electron. Informatics*, **4** (*1*) 1 (2020). doi:10.24843/JEEI.2020.v04.i01.p01.
27) B. Pranoto, I. Adilla, H. Soekarno, Nina Konitat Supriatna, Adrian, L. Efiyanti, Dian Anggraini Indrawan, Nurry Widya Hesty, and Silvy Rahmah Fithri, "Using satellite data of palm oil area for potential utilization in calculating palm oil trunk waste as cofiring fuel biomass," *Evergreen*, **10** (*3*) 1784–1791 (2023). doi:10.5109/7151728.
28) Y. Xu, K. Yang, J. Zhou, and G. Zhao, "Coal-biomass co-firing power generation technology: current status, challenges and policy implications," *Sustainability*, **12** (*9*) 3692 (2020). doi:10.3390/su12093692.
29) P. Basu, "Biomass Combustion and Cofiring," in: Biomass Gasification, Pyrolysis and Torrefaction, Elsevier, 2018: pp. 393–413. doi:10.1016/B978-0-12-812992-0.00011-X.
30) C.H. Lim, S.L. Ngan, W.P.Q. Ng, B.S. How, and H.L. Lam, "Biomass supply chain management and challenges," in: Value-Chain of Biofuels, Elsevier, 2022: pp. 429–444. doi:10.1016/B978-0-12-824388-6.00016-6.
31) A. Nuamah, A. Malmgren, G. Riley, and E. Lester, "Biomass Co-Firing," in: Compr. Renew. Energy, Elsevier, 2012: pp. 55–73. doi:10.1016/B978-0-08-087872-0.00506-0.
32) A. Demirbas, "Combustion characteristics of different biomass fuels," *Prog. Energy Combust. Sci.*, **30** (*2*) 219–230 (2004). doi:10.1016/j.pecs.2003.10.004.
33) J. Lalak, D. Martyniak, A. Kasprzycka, G. Żurek, W. Moroń, M. Chmielewska, D. Wiącek, and J. Tys, "Comparison of selected parameters of biomass and coal," *Int. Agrophysics*, **30** (*4*) 475–482 (2016). doi:10.1515/intag-2016-0021.
34) X. Meng, W. Zhou, E. Rokni, G. Chen, R. Sun, and Y.A. Levendis, "Release of alkalis and chlorine from combustion of waste pinewood in a fixed bed," *Energy & Fuels*, **33** (*2*) 1256–1266 (2019). doi:10.1021/acs.energyfuels.8b03970.
35) H.P. Nielsen, F.J. Frandsen, K. Dam-Johansen, and L.L. Baxter, "The implications of chlorine-associated corrosion on the operation of biomass-fired boilers," *Prog. Energy Combust. Sci.*, **26** (*3*) 283–298 (2000).

doi:10.1016/S0360-1285(00)00003-4.
36) B. Rahmanian, M.R. Safaei, S.N. Kazi, G. Ahmadi, H.F. Oztop, and K. Vafai, "Investigation of pollutant reduction by simulation of turbulent non-premixed pulverized coal combustion," *Appl. Therm. Eng.*, **73** (*1*) 1222–1235 (2014). doi:10.1016/j.applthermaleng.2014.09.016.
37) I.W. Agus Prasetyo Nuryadi, Chairunnisa Chairunnisa, Fitrianto Fitrianto, M.P. Helios, R.T. Soewono, R.J. Komara, "Simulation of turbulent non-premixed combustion in pulverized coal from kalimantan indonesia," *J. Polimesin*, **21** (*3*) 339–345 (2023). doi:10.30811/jpl.v21i3.3829.
38) C. Ghenai, and I. Janajreh, "CFD analysis of the effects of co-firing biomass with coal," *Energy Convers. Manag.*, **51** (*8*) 1694–1701 (2010). doi:10.1016/j.enconman.2009.11.045.
39) J. Li, A. Brzdekiewicz, W. Yang, and W. Blasiak, "Co-firing based on biomass torrefaction in a pulverized coal boiler with aim of 100% fuel switching," *Appl. Energy*, **99** 344–354 (2012). doi:10.1016/j.apenergy.2012.05.046.
40) M. Tamura, S. Watanabe, N. Kotake, and M. Hasegawa, "Grinding and combustion characteristics of woody biomass for co-firing with coal in pulverised coal boilers," *Fuel*, **134** 544–553 (2014). doi:10.1016/j.fuel.2014.05.083.
41) A. Milićević, S. Belošević, N. Crnomarković, I. Tomanović, A. Stojanović, D. Tucaković, Lei Deng, and D. Che, "Numerical study of co-firing lignite and agricultural biomass in utility boiler under variable operation conditions," *Int. J. Heat Mass Transf.*, **181** 121728 (2021). doi:10.1016/j.ijheatmasstransfer.2021.121728.
42) B.T.M. dan P. Tim, "Kajian Optimasi Boiler FTP Tahap 1 - Simulasi Menggunakan CFD. Report - No. 188-1/TPK-JTK/BTMP/10/13.," Jakarta, 2013.
43) M. Sijercic, S. Belosevic, and P. Stefanovic, "Modeling of pulverized coal combustion stabilization by means of plasma torches," *Therm. Sci.*, **9** (*2*) 57–72 (2005). doi:10.2298/TSCI0502057S.
44) T. Echekki, and E. Mastorakos, "Turbulent Combustion: Concepts, Governing Equations and Modeling Strategies," in: 2011: pp. 19–39. doi:10.1007/978-94-007-0412-1_2.
45) Z.Q. Li, F. Wei, and Y. Jin, "Numerical simulation of pulverized coal combustion and no formation," *Chem. Eng. Sci.*, **58** (*23–24*) 5161–5171 (2003). doi:10.1016/j.ces.2003.08.012.
46) S. Pirker, D. Kahrimanovic, and C. Goniva, "Improving the applicability of discrete phase simulations by smoothening their exchange fields," *Appl. Math. Model.*, **35** (*5*) 2479–2488 (2011). doi:10.1016/j.apm.2010.11.066.
47) B. Yan, Y. Cheng, Y. Jin, and C.Y. Guo, "Analysis of particle heating and devolatilization during rapid coal pyrolysis in a thermal plasma reactor," *Fuel Process. Technol.*, **100** 1–10 (2012). doi:10.1016/j.fuproc.2012.02.009.
48) T.-H. Shih, W.W. Liou, A. Shabbir, Z. Yang, and J. Zhu, "A new k-ϵ eddy viscosity model for high reynolds number turbulent flows," *Comput. Fluids*, **24** (*3*) 227–238 (1995). doi:10.1016/0045-7930(94)00032-T.
49) J.-K. Park, S. Park, M. Kim, C. Ryu, S.H. Baek, Y.J. Kim, H.H. Kim, and H.Y. Park, "CFD analysis of combustion characteristics for fuel switching to bioliquid in oil-fired power plant," *Fuel*, **159** 324–333 (2015). doi:10.1016/j.fuel.2015.06.079.
50) M. Goodarzi, M.R. Safaei, H.F. Oztop, A. Karimipour, E. Sadeghinezhad, M. Dahari, S.N. Kazi, and N. Jomhari, "Numerical study of entropy generation due to coupled laminar and turbulent mixed convection and thermal radiation in an enclosure filled with a semitransparent medium," *Sci. World J.*, **2014** 1–8 (2014). doi:10.1155/2014/761745.
51) W. Ding, Q. Eri, B. Kong, and Z. Zhang, "Numerical investigation of a compact tube heat exchanger for hypersonic pre-cooled aero-engine," *Appl. Therm. Eng.*, **170** 114977 (2020). doi:10.1016/j.applthermaleng.2020.114977.
52) W. Ding, Q. Eri, B. Kong, and C. Wang, "The effect of inlet pressure distortion on the performance of an axisymmetric compact tube heat exchanger with radial counter flow type for hypersonic pre-cooled aero-engine," *J. Mech. Sci. Technol.*, **36** (*6*) 3181–3191 (2022). doi:10.1007/s12206-022-0549-0.
53) S.R. Gubba, D.B. Ingham, K.J. Larsen, L. Ma, M. Pourkashanian, H.Z. Tan, A. Williams, and H. Zhou, "Numerical modelling of the co-firing of pulverised coal and straw in a 300mwe tangentially fired boiler," *Fuel Process. Technol.*, **104** 181–188 (2012). doi:10.1016/j.fuproc.2012.05.011.
54) I. Constenla, J.L. Ferrín, and L. Saavedra, "Numerical study of a 350mwe tangentially fired pulverized coal furnace of the as pontes power plant," *Fuel Process. Technol.*, **116** 189–200 (2013). doi:10.1016/j.fuproc.2013.05.016.
55) A.H. Al-Abbas, J. Naser, and E.K. Hussein, "Numerical simulation of brown coal combustion in a 550 mw tangentially-fired furnace under different operating conditions," *Fuel*, **107** 688–698 (2013). doi:10.1016/j.fuel.2012.11.054.
56) Z.F. Tian, P.J. Witt, M.P. Schwarz, and W. Yang, "Numerical modeling of victorian brown coal combustion in a tangentially fired furnace," *Energy & Fuels*, **24** (*9*) 4971–4979 (2010). doi:10.1021/ef100514v.
57) Y. Fei, S. Black, J. Szuhánszki, L. Ma, D.B. Ingham, P.J. Stanger, and M. Pourkashanian, "Evaluation of the potential of retrofitting a coal power plant to oxy-firing using cfd and process co-simulation," *Fuel Process. Technol.*, **131** 45–58 (2015). doi:10.1016/j.fuproc.2014.10.042.

58) M.P. Helios, A. Maswan, A.M. Fathoni, H. Sutriyanto, and W. Asvapoositkul, "Numerical study effect of throat shape to energy dissipation in water jet pump via entropy generation analysis," in: 2023: p. 050017. doi:10.1063/5.0112723.

59) F. Karuana, H. Ghazidin, Suyatno, A.R. Wimada, M.P. Helios, H. Sutriyanto, and M.D. Solikhah, "Homogeneity analysis of B30 mixing results with additives in mixing tanks using computational fluid dynamics (CFD)," in: Mater. Today Proc., 2023: pp. 141–146. doi:10.1016/j.matpr.2023.02.388.

60) J.S. Chandok, I.N. Kar, and S. Tuli, "Estimation of furnace exit gas temperature (fegt) using optimized radial basis and back-propagation neural networks," *Energy Convers. Manag.*, **49** (*8*) 1989–1998 (2008). doi:10.1016/j.enconman.2008.03.011.

61) M.S. Ray, "Boilers, evaporators and condensers, by s. kacak. john wiley and sons, inc., new york, usa (1991). 835 pp. isbn 0471-62170-6.," *Dev. Chem. Eng. Miner. Process.*, **1** (*1*) 64–65 (1993). doi:10.1002/apj.5500010110.

62) A.P. Nuryadi, M.P. Helios, A.M. Fathoni, C. Chairunnisa, F. Fitrianto, H. Pujowidodo, K.P. Sumarah, R.J. Komara, F.M. Kuswa, and R.T. Soewono, "Simulasi cfd pengurangan co2 pada co-firing batubara dan tandan kosong kelapa sawit menggunakan model pembakaran non-premixed," *J. Teknol. Lingkung.*, **24** (*2*) 283–291 (2023). doi:10.55981/jtl.2023.725.

63) A.P. Nuryadi, R.J. Komara, M.P. Helios, I. Wulandari, C. Chairunnisa, and F. Fitrianto, "CFD simulation of oxy-fuel combustion using turbulent non-premixed combustion with medium-rank coal from kalimantan indonesia," *J. Polimesin*, **21** (*04*) (2023). doi:10.30811/jpl.v21i4.3830.

64) Hariana, A. Prismantoko, G.A. Ahmadi, and A. Darmawan, "Ash evaluation of indonesian coal blending for pulverized coal-fired boilers," *J. Combust.*, **2021** 1–15 (2021). doi:10.1155/2021/8478739.

65) S. Nozawa, N. Wada, Y. Matsushita, T. Yamamoto, M. Oomori, and T. Harada, "Experimental and numerical investigation of effect of coal rank on burn-off time in pulverized coal combustion," *Evergr. - Jt. J. Nov. Carbon Resour. Sci. Green Asia Strateg.*, **5** 23–27 (2012).

66) M. Kumar, and S.K. Patel, "The characteristics and power generation energetics of coal, cattle dung, rice husk, and their blends," *Energy Sources, Part A Recover. Util. Environ. Eff.*, **36** (*7*) 700–708 (2014). doi:10.1080/15567036.2010.545798.

67) J. Blondeau, J. Van den Auweele, S. Alimuddin, F. Binder, and F. Turoni, "Online adjustment of furnace exit gas temperature field using advanced infrared pyrometry: case study of a 1500 mw utility boiler," *Case Stud. Therm. Eng.*, **21** 100649 (2020). doi:10.1016/j.csite.2020.100649.

68) Halim, and A.B.K. Putra, "Numerical Study of the Effects of Burner Tilt and Coal Optimization on Combustion Characteristics of 350 MWe Tangentially Fired Pulverized Coal Boiler," in: 2022: pp. 303–310. doi:10.1007/978-981-19-1581-9_34.

69) B. Yang, Y.-M. Wei, L.-C. Liu, Y.-B. Hou, K. Zhang, L. Yang, and Y. Feng, "Life cycle cost assessment of biomass co-firing power plants with co2 capture and storage considering multiple incentives," *Energy Econ.*, **96** 105173 (2021). doi:10.1016/j.eneco.2021.105173.

70) Z. Luo, and J. Zhou, "Thermal Conversion of Biomass," in: Handb. Clim. Chang. Mitig. Adapt., Springer New York, New York, NY, 2021: pp. 1–57. doi:10.1007/978-1-4614-6431-0_27-3.

71) J. Chang, Z. Zhou, X. Ma, and J. Liu, "Computational investigation of hydrodynamics, coal combustion and nox emissions in a tangentially fired pulverized coal boiler at various loads," *Particuology*, **65** 105–116 (2022). doi:10.1016/j.partic.2021.06.012.

72) Y. Wang, Y. Sun, M. Yue, and Y. Li, "Reaction kinetics of chlorine corrosion to heating surfaces during coal and biomass cofiring," *J. Chem.*, **2020** 1–10 (2020). doi:10.1155/2020/2175795.

73) D. Schmid, O. Karlström, and P. Yrjas, "Release of nh3, hcn and no during devolatilization and combustion of washed and torrefied biomass," *Fuel*, **280** 118583 (2020). doi:10.1016/j.fuel.2020.118583.

74) P. Glarborg, "Fuel nitrogen conversion in solid fuel fired systems," *Prog. Energy Combust. Sci.*, **29** (*2*) 89–113 (2003). doi:10.1016/S0360-1285(02)00031-X.

75) L.-N. Wu, Z.-Y. Tian, W. Qin, X.-Y. Hu, and C.-Q. Dong, "Understanding the effect of cao on hcn conversion and nox formation during the circulating fluidized combustion process using dft calculations," *Proc. Combust. Inst.*, **38** (*4*) 5355–5362 (2021). doi:10.1016/j.proci.2020.08.023.

76) P. Glarborg, J.A. Miller, B. Ruscic, and S.J. Klippenstein, "Modeling nitrogen chemistry in combustion," *Prog. Energy Combust. Sci.*, **67** 31–68 (2018). doi:10.1016/j.pecs.2018.01.002.

77) H.-G. Bachmann, "Prevention of biodeterioration of wooden objects of art: influence of fumigation with hydrocyanic acid on metals," *Stud. Conserv.*, **26** (*3*) 111 (1981). doi:10.2307/1505852.

78) A. Wahid, R. Mustafida, and A. Husnil, "Exergy analysis of coal-fired power plants in ultra supercritical technology versus integrated gasification combined cycle," *Evergreen*, **7** (*1*) 32–42 (2020). doi:10.5109/2740939.